Applied Catalysis B: Environmental 86 (2009) 114–120

Contents lists available at ScienceDirect

Applied Catalysis B: Environmental

journal homepage: www.elsevier.com/locate/apcatb

# Selective steam reforming of methanol over silica-supported copper catalyst prepared by sol–gel method

Yasuyuki Matsumura [a,*], Hideomi Ishibe [b]

[a] National Institute of Advanced Industrial Science and Technology (AIST), Kansai Center, Midorigaoka, Ikeda, Osaka 563-8577, Japan
[b] Nippon Seisen Co., Ltd., Hirakata Plant, Ikenomiya, Hirakata, Osaka 573-8522, Japan

ARTICLE INFO

*Article history:*
Received 31 March 2008
Received in revised form 11 August 2008
Accepted 14 August 2008
Available online 22 August 2008

*Keywords:*
Methanol steam reforming
Copper supported on silica
Sol–gel method
CO formation
X-ray diffraction
X-ray photoelectron spectroscopy

ABSTRACT

Silica-supported copper prepared by a sol–gel method can selectively catalyze methanol steam reforming to hydrogen and carbon dioxide at 250 °C. The catalytic activity increases with the copper content up to 40 wt.%. The selectivity to carbon monoxide with the catalysts containing 20–40 wt.% of copper is significantly lower than that with a commercial $Cu/ZnO/Al_2O_3$ catalyst. Copper particles are highly dispersed in the catalyst whose Cu content is 20 wt.% or less. After the reaction at 250 °C the particles are present as $Cu_2O$ with the mean crystallite size less than 4 nm. In the catalyst with the Cu content of 30–50 wt.%, the fine $Cu_2O$ particles coexist with large metallic Cu particles whose mean crystallite size is 30–40 nm after the reaction. The large metallic particles are supposed to contribute to the reaction as well as the fine $Cu_2O$ particles although the surface area is estimated to be significantly smaller than that of the latter.



## 1. Introduction

The hydrogen production by steam reforming of methanol is one of the key issues for the development of fuel cell powered devices such as electric vehicles. Polymer electrolyte fuel cells (PEFCs) are generally employed for the mobile applications while the hydrogen fuel must not contain carbon monoxide above 10 ppm, which poisons the catalytic anode [1]. Copper catalysts such as $Cu/ZnO/Al_2O_3$ are usually selective in the steam reforming to hydrogen and carbon dioxide ($CH_3OH + H_2O \rightarrow 3H_2 + CO_2$), but additional reactors are required in the fuel processor system to remove by-produced carbon monoxide to the level less than 10 ppm [2]. Selective oxidation of carbon monoxide is often carried out to remove carbon monoxide from the reforming gas [1], although an excessive amount of oxygen is required in the process. Hence, high CO concentration causes loss of hydrogen and additional reactors to the reformer. Membrane separation of hydrogen is attractive because pure hydrogen is obtained through a pinhole-free palladium membrane [3]. However, defects usually exist on thin membranes and they decrease the selectivity ratio of hydrogen to other gases. For example, when the ratio is as high as 1000 and the CO concentration in the reforming gas is 1.2%, which is produced in the reforming with steam/methanol molar ratio of 1.5 under the equilibrium at 250 °C and at 1 MPa, 18 ppm of carbon monoxide is still present in the permeated hydrogen. This insufficient CO concentration requires addition of CO removal process such as methanation ($CO + 3H_2 \rightarrow CH_4 + H_2O$) to the hydrogen processor for PEFC. Hence, prevention of CO by-production is important for simplification of the system even if it equips a hydrogen permeable membrane.

Agrell et al. reported that CO by-production is caused by the reverse water–gas shift reaction ($CO_2 + H_2 \rightarrow CO + H_2O$) in the methanol steam reforming over $Cu/ZnO/Al_2O_3$, which is also active to the reverse water–gas shift reaction [4]. Copper supported on silica is also active to the methanol steam reforming [5], while the activity toward water–gas shift reaction is sensitive to the structure such as the particle size of copper [6]. Since copper particles can be highly dispersed in $Cu/SiO_2$ prepared by a sol–gel method [7], we have employed the sol–gel method in preparation of $Cu/SiO_2$ with the Cu content up to 50 wt.% and examined the activity to the methanol steam reforming. Here, it is shown that the selectivity to carbon monoxide is low in the reaction over the $Cu/SiO_2$ catalysts at 250 °C.

## 2. Experimental

Silica-supported copper catalysts ($x$-$Cu/SiO_2$, $x$ represents the copper content in wt.%) were prepared by the hydrolysis and

* Corresponding author. Tel.: +81 72 751 7821; fax: +81 72 751 9623.
*E-mail address:* yasu-matsumura@aist.go.jp (Y. Matsumura).

0926-3373/$ – see front matter © 2008 Elsevier B.V. All rights reserved.
doi:10.1016/j.apcatb.2008.08.007

polymerization of a mixture of tetramethoxy silane (Tokyo Chemical Industry), copper nitrate (Wako, S-grade), water, and methanol at room temperature for 1 day. After drying in air at 120 °C they were heated in air for 5 h at 500 °C for removal of $NO_3^-$ anions and residual organic compounds. A commercial $Cu/ZnO/Al_2O_3$ catalyst (Süd-Chemie, MDC-3), which is reported to be durable in the reaction even at 350 °C [8], was used as a reference.

Catalytic tests were performed in a fixed-bed continuous-flow reactor operated under atmospheric pressure. A catalyst (0.50 g, granules of 10–20 mesh) was placed in a tube reactor made of stainless steel (i.d., 7 mm). After the pre-reduction in a stream of 15 vol.% hydrogen diluted with argon (3.5 $dm^3\ h^{-1}$) at a desired temperature for 1 h, a mixture of methanol, steam, and argon (1.0/1.5/1.0 in molar ratio) was introduced at 250 or 300 °C with a flow rate of 10.6 $dm^3\ h^{-1}$. The effluent gas was dried with a cold trap at ca. −50 °C, and analyzed with an on-stream gas chromatograph (Shimadzu GC-8A; activated carbon, 2 m; Ar carrier) equipped with a thermal conductivity detector. The methanol conversion was determined from the material balance of the reactant and the products, and the error was within 5%. No formation of formaldehyde, methane or methyl formate was observed.

The BET surface areas of the catalysts were determined from the isotherms of nitrogen physisorption.

Powder XRD (X-ray diffraction) patterns of the catalysts were recorded in air at room temperature with an MAC Science MP6XCE diffractometer using nickel-filtered Cu Kα radiation. The Rietveld refinement of the patterns was carried out using the Rietveld software RIETAN-2000 [9]. To obtain the quantitative phase abundance, the XRD data of 30–70° in two theta were modeled with monoclinic CuO (space group, *C2/c*), cubic $Cu_2O$ (*Pn*-3*m*), and cubic Cu (*Fm*-3*m*) using a pseudo-Voigt function. The factor of $R_{wp}$ was always less than 5%.

X-ray photoelectron spectra (XPS) were recorded at room temperature with a JEOL JPS-9010MX spectrometer (Mg Kα). The sample was taken out from the reactor after cooling under an argon stream for 12 h or longer and mounted in air to a sample holder. Binding energies were corrected by the reference of the C 1s line at 284.6 eV. The surface atomic concentrations of Cu, Si, and O were calculated from the peak areas using the atomic relative sensitivity factors (ARSF) of Cu $2p_{3/2}$ (13), Si 2p (1.0), and O 1s (2.4) determined by measuring standard materials of copper plate, silicon wafer, and quartz glass plate. The concentration analysis using ARSF is quantitative and the uncertainty is less than 2% [10].

Temperature-programmed reduction (TPR) of the catalyst (0.50 g) was carried out in a stream of 15 vol.% hydrogen diluted with argon at a flow rate of 3.5 $dm^3\ h^{-1}$. Temperature of the sample bed was risen linearly at a rate of 200 °C $h^{-1}$. The hydrogen consumption was monitored by analyzing the hydrogen concentration with the on-stream GC every 3 min. No complete hydrogen consumption was observed in the reduction.

## 3. Results

### 3.1. Methanol steam reforming over silica-supported copper

Steam reforming of methanol was carried out over the silica-supported copper catalyst. Hydrogen and carbon dioxide were almost quantitatively formed at 250 °C, while a small amount of carbon monoxide was by-produced. The activity of the catalyst pre-reduced at 250 °C increased with an increase in the copper content up to 40 wt.%, but decreased at 50 wt.% (Fig. 1). Interestingly, the selectivity to carbon monoxide was reversely decreased to 0.10% at 40 wt.%. The activity at 250 °C gradually decreased with the time-on-stream, but the decrease was not obvious after 4 h on-stream (Fig. 2). The activity of a commercial

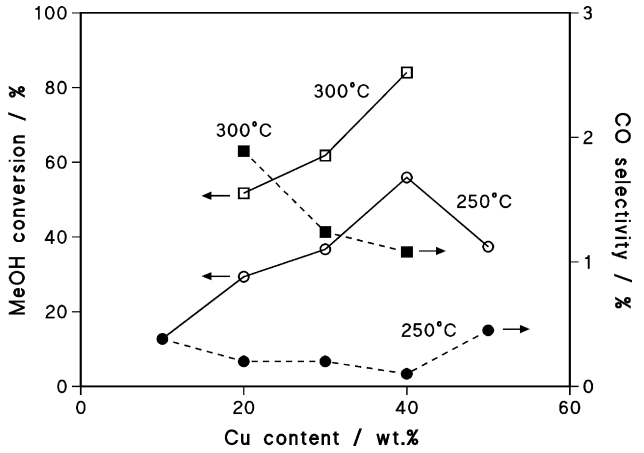


**Fig. 1.** Catalytic activity of $Cu/SiO_2$ prepared by a sol–gel method in methanol steam reforming after 6 h. Pre-reduction temperatures are the same as the reaction temperatures shown in the figure.

$Cu/ZnO/Al_2O_3$ catalyst at 250 °C was significantly lower than that of 40-$Cu/SiO_2$, and the selectivity to carbon monoxide was as high as 0.47%. The pre-reduction temperature of 40-$Cu/SiO_2$ affected its activity and selectivity. That is, the higher pre-reduction temperature of 300 or 400 °C caused less activity. It is noteworthy that no carbon monoxide was detected in the products, showing that the selectivity to carbon monoxide was less than 0.03% (Fig. 3). The activity of $Cu/ZnO/Al_2O_3$ increased appreciably with an increase in the reduction temperature, but the CO selectivity also increased.

When the reaction was carried out at 300 °C, the activities of $Cu/SiO_2$ increased in parallel manner with those at 250 °C (see Fig. 1). The activity decreased gradually with an increase in the time-on-stream (see Fig. 2). For example, the methanol conversion with 40-$Cu/SiO_2$ pre-reduced at 300 °C was 95% at 1 h-on-stream and it was 84% at 6 h-on-stream. The selectivity of carbon monoxide was 1.1% throughout the reaction. When a double amount of the catalyst was used, the conversion was 97% at 1 h-on-stream and the CO selectivity increased to 2.0%. In the case of $Cu/ZnO/Al_2O_3$ at 300 °C, the selectivity to carbon monoxide was 1.1%, but the activity was considerably lower than that of 40-$Cu/SiO_2$ (see Fig. 2).

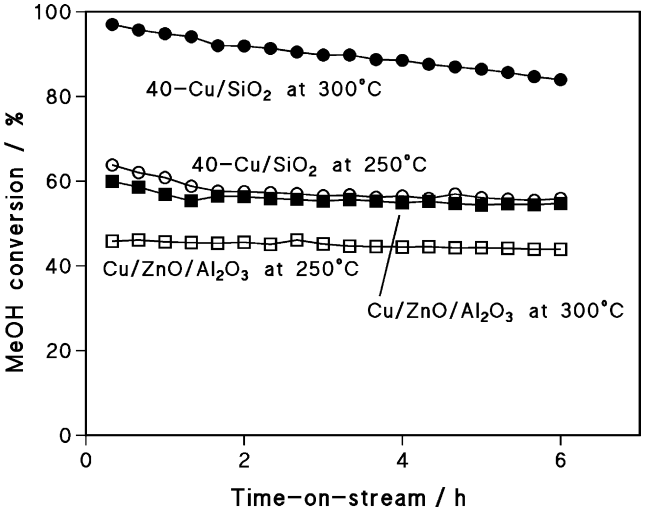


**Fig. 2.** Comparison of the catalytic activity of 40-$Cu/SiO_2$ to that of a commercial $Cu/ZnO/Al_2O_3$. Pre-reduction temperatures are the same as the reaction temperatures shown in the figure.

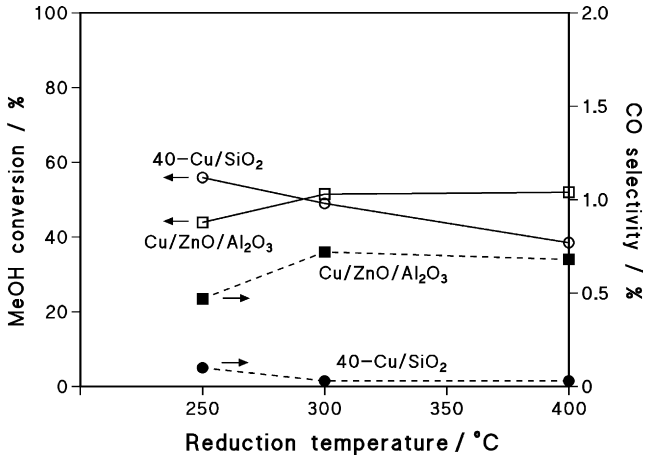


**Fig. 3.** Catalytic acitivity of 40-Cu/$SiO_2$ and Cu/ZnO/$Al_2O_3$ with different reduction temperatures in the reaction at 250 °C after 6 h.

### 3.2. Physical properties of catalysts after reaction

A weak peak at 43.3° in 2$\theta$ assigned to Cu(1 1 1) was recorded with a slight peak at 37° assigned to $Cu_2O$(1 1 1) in the XRD pattern for 10-Cu/$SiO_2$ just after reduction at 250 °C (Fig. 4a) [11]. After the reaction at 250 °C a broad peak at 36.7° assigned to $Cu_2O$(1 1 1) was recorded with a slight peak at 42° assigned to $Cu_2O$(2 0 0) in the XRD pattern (Fig. 4b) [11]. The peaks attributed to $Cu_2O$ were intensified in the pattern for 20-Cu/$SiO_2$ with a very small peak at 43.4°. The pattern changed drastically when the Cu content was 30 wt.% or above, that is, the peaks at 43.4° and 50.5° attributed to metallic copper appeared clearly with a weak peak at 36.7° attributed to $Cu_2O$. Mean crystallite sizes were determined from the line broadening of the XRD peaks of Cu(1 1 1) and $Cu_2O$(1 1 1) using Scherrer equation [12]; in the cases of metal or metal oxide particles dispersed on supports, the crystallite size is usually close to the mean particle size [13,14]. The crystallite sizes for metallic copper particles on Cu/$SiO_2$ containing 30–50 wt.% Cu were 31–39 nm, and those for $Cu_2O$ were 4–7 nm for the catalysts containing 10–50 wt.% Cu (Table 1). The atomic ratios of Cu in $Cu_2O$ to that in Cu metal determined by the Rietveld analysis were 0.3 for 30-Cu/$SiO_2$, 0.3 for 40-Cu/$SiO_2$, and 0.07 for 50-Cu/$SiO_2$.

**Table 1**
Physical properties of the catalysts after methanol steam reforming at 250 °C for 6 h

| Catalyst | Reduction temperature (°C) | BET surface area ($m^2\ g^{-1}$) | Crystallite size (nm) | |
|---|---|---|---|---|
| | | | $Cu_2O$ | Cu |
| 10-Cu/$SiO_2$[a] | 250 | | 3 | 5 |
| 10-Cu/$SiO_2$ | 250 | 292 | 4 | – |
| 20-Cu/$SiO_2$ | 250 | 376 | 4 | – |
| 30-Cu/$SiO_2$ | 250 | 345 | 5 | 34 |
| 40-Cu/$SiO_2$ | 250 | 345 | 5 | 31 |
| 40-Cu/$SiO_2$ | 300 | 320 | 4 | 36 |
| 40-Cu/$SiO_2$ | 400 | 341 | 4 | 36 |
| 40-Cu/$SiO_2$[a] | 400 | | – | 37 |
| 40-Cu/$SiO_2$[b] | 300 | 316 | 4 | 32 |
| 50-Cu/$SiO_2$ | 250 | 250 | 7 | 39 |
| 50-Cu/$SiO_2$[a] | 250 | | – | 39 |

[a] Just after reduction with hydrogen.
[b] After reaction at 300 °C for 6 h.

The XRD peak at 36.7° assigned to $Cu_2O$(1 1 1) was insignificant with 40-Cu/$SiO_2$ just after the reduction at 400 °C, while the peak was present in the pattern for the catalyst after the reaction regardless of the pre-reduction temperature (Fig. 5). The crystallite size of metallic copper for 40-Cu/$SiO_2$ pre-reduced at 300 or 400 °C after the reaction at 250 °C was discernibly larger than that pre-reduced at 250 °C (see Table 1).

The BET surface areas for the catalysts after the reaction at 250 °C were 250–376 $m^2\ g^{-1}$ (see Table 1).

### 3.3. XPS of the copper catalysts after the reaction

The surface of Cu/$SiO_2$ after the reaction at 250 °C was characterized by XPS. The binding energy of Cu $2p_{3/2}$ for 10-Cu/$SiO_2$ was 933.2 eV and appreciably higher than 932.4 eV attributed to metallic copper or $Cu_2O$ (Fig. 6a and Table 2) [15]. In order to identify the electronic state, the Auger line of Cu $L_3VV$ was recorded (Fig. 7a). The kinetic energy was 915.5 eV which is lower than that for $Cu_2O$ at 916.8 eV [15]. The energy for Cu metal is 918.7 eV [15]. The $\alpha$ value (Auger parameter + photon energy) was 1848.7 eV being lower than 1849.4 eV for $Cu_2O$ and 1851.3 eV for

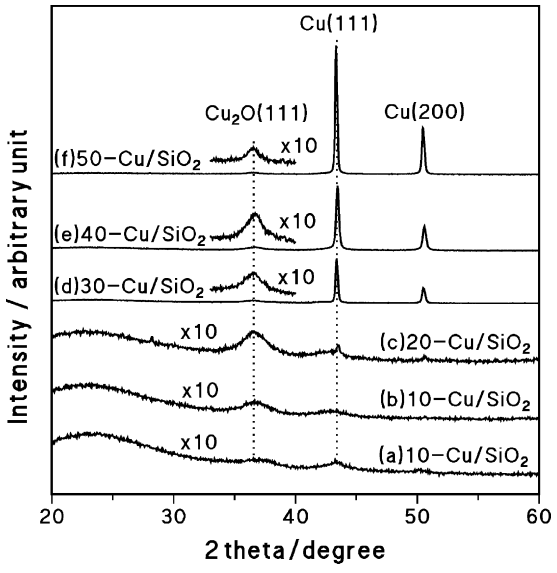


**Fig. 4.** XRD patterns of Cu/$SiO_2$. (a) 10-Cu/$SiO_2$ reduced at 250 °C and (b–f) Cu/$SiO_2$ after the reaction at 250 °C for 6 h following the reduction at 250 °C.

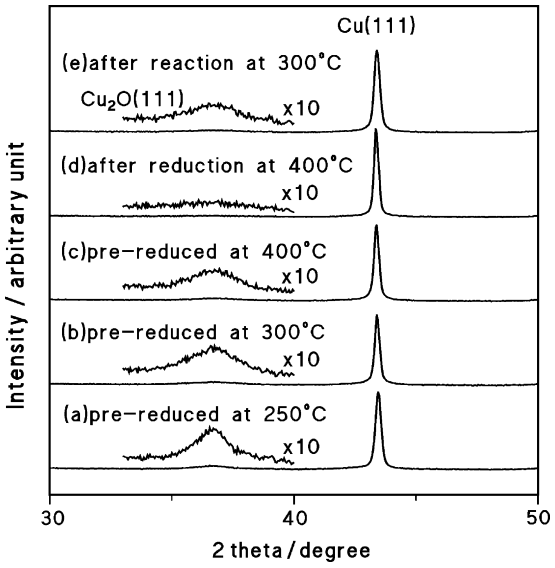


**Fig. 5.** XRD patterns of 40-Cu/$SiO_2$. (a–c) After the reaction at 250 °C, (d) just after the reduction at 400 °C, and (e) after the reaction at 300 °C following the reduction at 300 °C.

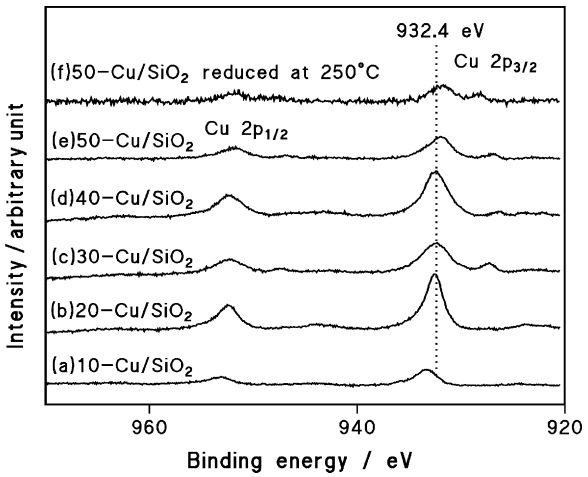


**Fig. 6.** XPS of Cu 2p region for $Cu/SiO_2$. (a–e) After the reaction at 250 °C following the reduction at 250 °C, and (f) after the reduction at 250 °C.

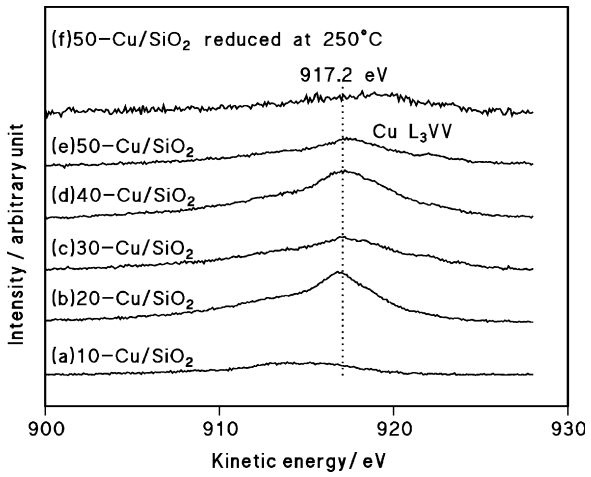


**Fig. 7.** Auger line of Cu $L_3VV$ for $Cu/SiO_2$. (a–e) After the reaction at 250 °C following the reduction at 250 °C, and (f) after the reduction at 250 °C.

metallic copper, while the $\alpha$ value for CuO is 1851.7 eV [15]. The $\alpha$ value for 10-$Cu/SiO_2$ just after reduction at 250 °C was 1849.6 eV and significantly higher than that for the catalyst after the reaction (see Table 2). The energy of Cu $2p_{3/2}$ for 20-$Cu/SiO_2$ was 932.4 eV and the $\alpha$ value was 1849.2 eV, showing presence of $Cu_2O$ on the surface. The similar values were recorded with 30, 40, and 50-$Cu/SiO_2$ (see Table 2). The $\alpha$ value for 50-$Cu/SiO_2$ just after the reduction with hydrogen at 250 °C was 1850.5 eV that is in the middle of those for $Cu_2O$ and metallic copper.

The pre-reduction temperatures of 250–400 °C did not significantly affect the energies of Cu $2p_{3/2}$ and Cu $L_3VV$ for 40-$Cu/SiO_2$, while the Auger line just after the reduction at 400 °C was at 918.0 eV (Figs. 8 and 9). The binding energy of Cu $2p_{3/2}$ for 40-$Cu/SiO_2$ after the reaction at 300 °C following the reduction at 300 °C was discernibly higher than that after the reaction at 250 °C, while the $\alpha$ values were close to each other (see Table 2).

The $\alpha$ value for 40-$Cu/SiO_2$ just after the reduction at 400 °C was 1850.5 eV, which is the same as that for 50-$Cu/SiO_2$ reduced at 250 °C.

The binding energies of O 1s and Si 2p were $533.0 \pm 0.1$ and $103.4 \pm 0.2$ eV, respectively, regardless of the samples. The surface atomic composition of Cu, Si, and O is also given in Table 2.

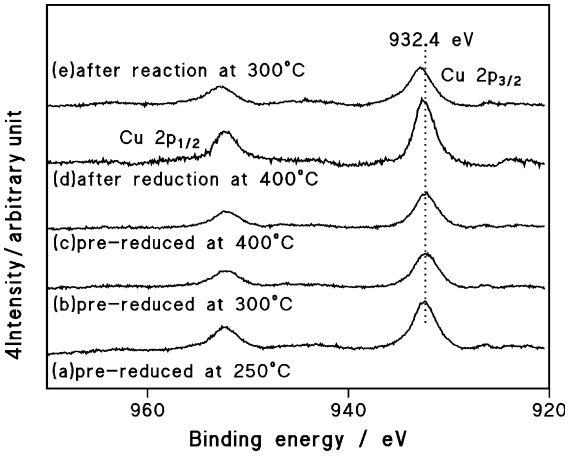


**Fig. 8.** XPS of Cu 2p region for 40-$Cu/SiO_2$. (a–c) After the reaction at 250 °C, (d) just after the reduction at 400 °C, and (e) after the reaction at 300 °C following the reduction at 300 °C.

### 3.4. TPR of copper catalysts

Reduction of $Cu/SiO_2$ catalysts started at ca. 150 °C in TPR experiments regardless of the Cu content (Fig. 10). The maxima of the reduction peaks for 10 and 20-$Cu/SiO_2$ were at around 190 °C, but another peak was present at around 230 °C in the profile of 30-$Cu/SiO_2$. Broad peaks were observed at around 200 and 210 °C with 40 and 50-$Cu/SiO_2$, respectively. The molar amounts of

**Table 2**
Summery of the XPS data for the catalysts after methanol steam reforming at 250 °C for 6 h

| Catalyst | Reduction temperature (°C) | Cu $2p_{3/2}$ (eV) | Cu $L_3VV$ (eV) | $\alpha$ (eV) | Surface atomic composition (%) | | |
|---|---|---|---|---|---|---|---|
| | | | | | Cu | Si | O |
| 10-$Cu/SiO_2$ | 250 | 933.2 | 915.5 | 1848.7 | 2 | 25 | 73 |
| 10-$Cu/SiO_2$[a] | 250 | 933.2 | 916.4 | 1849.6 | 2 | 25 | 73 |
| 20-$Cu/SiO_2$ | 250 | 932.4 | 916.8 | 1849.2 | 5 | 19 | 76 |
| 30-$Cu/SiO_2$ | 250 | 932.4 | 917.0 | 1849.4 | 4 | 21 | 75 |
| 40-$Cu/SiO_2$ | 250 | 932.4 | 917.1 | 1849.5 | 6 | 18 | 76 |
| 40-$Cu/SiO_2$ | 300 | 932.4 | 917.2 | 1849.6 | 4 | 21 | 75 |
| 40-$Cu/SiO_2$ | 400 | 932.3 | 917.2 | 1849.5 | 4 | 23 | 73 |
| 40-$Cu/SiO_2$[a] | 400 | 932.5 | 918.0 | 1850.5 | 5 | 22 | 73 |
| 40-$Cu/SiO_2$[b] | 300 | 932.7 | 916.9 | 1849.6 | 5 | 20 | 75 |
| 50-$Cu/SiO_2$ | 250 | 932.1 | 917.4 | 1849.5 | 2 | 25 | 73 |
| 50-$Cu/SiO_2$[a] | 250 | 931.8 | 918.7 | 1850.5 | 3 | 21 | 76 |

[a] Just after reduction with hydrogen.
[b] After reaction at 300 °C for 6 h.

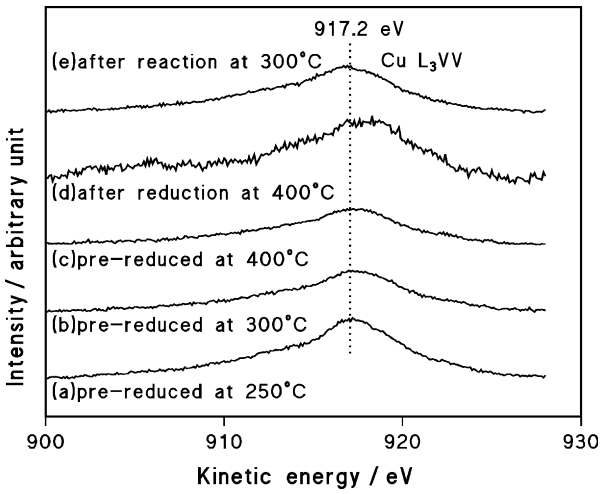


**Fig. 9.** Auger line of Cu $L_3VV$ for 40-Cu/$SiO_2$. (a–c) After the reaction at 250 °C, (d) just after the reduction at 400 °C, and (e) after the reaction at 300 °C following the reduction at 300 °C.

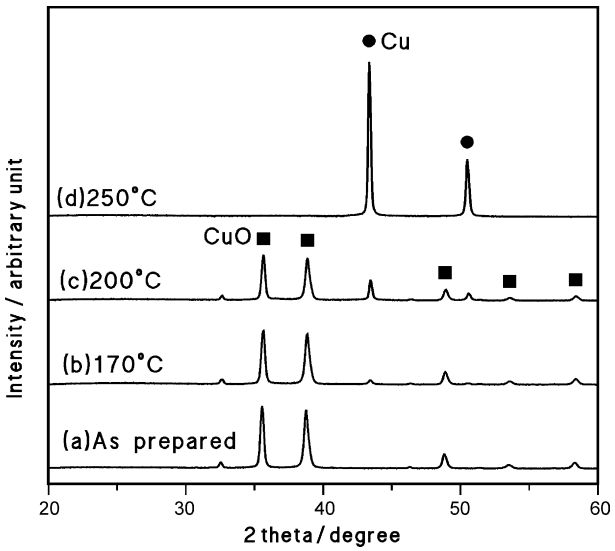


**Fig. 11.** XRD of 50-Cu/$SiO_2$. (a) As prepared, (b) reduced up to 170 °C in TPR, (c) reduced up to 200 °C in TPR, and (d) reduced at 250 °C for 1 h.

hydrogen consumed corresponded well to the molar contents of copper in the catalysts, showing complete reduction of CuO in the catalysts.

The XRD peaks in the pattern of 50-Cu/$SiO_2$ as prepared were attributed to CuO (Fig. 11a), while the mean crystallite size was 24 nm on the basis of the line broadening of the peak at 48.8° [12]. In a TPR experiment, 50-Cu/$SiO_2$ was reduced up to 170 °C and quenched under an argon stream, while ca. 1 m mol $g^{-1}$ of $H_2$ was consumed. Small peaks attributed to metallic Cu were recorded in the XRD pattern of the sample after the reduction up to 170 °C (Fig. 11b). The mean crystallite size of Cu was 29 nm. The $H_2$ consumption was ca. 3 m mol $g^{-1}$ in the reduction up to 200 °C followed by quenching. The intensity of the XRD peaks attributed to metallic copper increased in the pattern for the sample (Fig. 11c), but the peaks attributed to CuO were major. The mean crystallite size of Cu was 34 nm. The molar fractions of Cu/(Cu + CuO) determined by the Rietveld analysis were 4 and 15% in the reduction up to 170 and 200 °C, respectively. Only the peaks attributed to metallic copper were recorded in the XRD pattern for the sample reduced at 250 °C for 1 h, while the mean crystallite size was 39 nm (Fig. 11d).

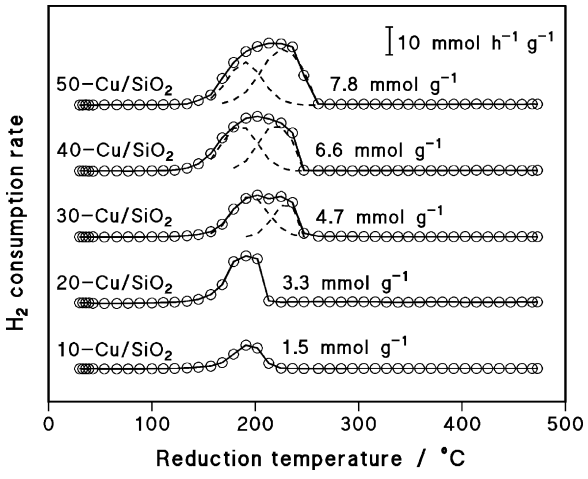


**Fig. 10.** Profiles of temperature-programmed reduction for Cu/$SiO_2$ with the heating rate of 200 °C $h^{-1}$. Total consumption amounts of $H_2$ are given in the figure.

## 4. Discussion

### 4.1. State of Cu particles on Cu/$SiO_2$ prepared by sol–gel method

The XRD patterns for 10-Cu/$SiO_2$ after the reduction with hydrogen at 250 °C (see Fig. 4a) shows presence of $Cu_2O$ and metallic Cu. Since the TPR result evidences almost complete reduction of the catalyst by heating up to 250 °C, the fine Cu particles are partly oxidized to $Cu_2O$ during the handling in air. On the other hand, no metallic Cu can be seen in the pattern of the catalyst after the reaction for 6 h (see Fig. 4b). Hence, the oxidation state of the catalyst after the reaction is different from that just after the reduction, and it is suggested that at least the major part of the fine Cu particles is already oxidized in the reaction. In the XPS analysis the $\alpha$ value usually depends on the oxidation state of copper [15]. Since the value for 10-Cu/$SiO_2$ just after the reduction is lower than that of metallic copper, it is evident that the Cu surface is oxidized in air. However, the $\alpha$ value for the catalyst after the reaction is significantly lower than that after the reduction at 250 °C (see Table 2), showing that the degree of oxidation after the reaction is deeper than just after the reduction. Thus, the XPS result agrees that the surface of the fine Cu particles is already oxidized during the reaction. It is known that metallic nickel particles are oxidized on a silica support in the steam reforming of methane at 500 °C [16], suggesting that silica can promote oxidation of metallic particles in the presence of steam.

In the cases of 30-, 40- and 50-Cu/$SiO_2$, the XRD patterns show coexistence of $Cu_2O$ and metallic Cu after the reaction (see Figs. 4 and 5), but the $\alpha$ values are close to that of $Cu_2O$ (see Table 2). The values are not mainly due to the oxidation of the metallic Cu particles with the handling in air because the values for the catalysts just after the reduction are significantly higher than those after the reaction.

The XRD pattern of 30-Cu/$SiO_2$ evidences presence of fairly large Cu particles (see Fig. 4d). The TPR profile for 30-Cu/$SiO_2$ can be deconvoluted to two peaks (see Fig. 10). The position of the peak at the lower temperature is similar to those for 10 and 20-Cu/$SiO_2$, suggesting presence of fine CuO particles before the reduction. In actual, a small and broad peak attributed to $Cu_2O$ is present in the XRD pattern for 30-Cu/$SiO_2$ after the reaction. On the basis of the hydrogen consumption in the TPR of 50-Cu/$SiO_2$, it is evaluated that ca. 10% of CuO is reduced at 170 °C and ca. 40% at 200 °C.

**Table 3**
Estimation of the quantity of copper atoms on the catalyst surface

| Catalyst[a] | Surface Cu atom[b] (m mol $g^{-1}$) | Cu of fine particles (m mol $g^{-1}$) | | Cu of large particles (m mol $g^{-1}$) | |
|---|---|---|---|---|---|
| | | Surface | Total | Surface | Total |
| 10-Cu/$SiO_2$ | 0.4 | 0.8 | 1.6 | 0 | 0 |
| 20-Cu/$SiO_2$ | 1.5 | 1.7 | 3.1 | 0 | 0 |
| 30-Cu/$SiO_2$ | 0.9 | 1.3 | 2.9 | 0.07 | 1.8 |
| 40-Cu/$SiO_2$ | 1.5 | 1.4 | 3.1 | 0.14 | 3.1 |
| 40-Cu/$SiO_2$[c] | 1.0 | 1.7 | 3.1 | 0.12 | 3.1 |
| 40-Cu/$SiO_2$[d] | 0.9 | 1.7 | 3.1 | 0.12 | 3.1 |
| 50-Cu/$SiO_2$ | 0.4 | 0.9 | 3.0 | 0.17 | 4.9 |

[a] Reduced with hydrogen at 250 °C except otherwise mentioned.
[b] The number of Cu atoms on the catalyst surface after the reaction at 250 °C.
[c] Reduced with hydrogen at 300 °C.
[d] Reduced with hydrogen at 400 °C.

However, the intensity of the XRD peaks attributed to large Cu particles is small (see Fig. 11). The reducibilities determined by the Rietveld analysis on the XRD in Fig. 11b and c are 4% at 170 °C and 15% at 200 °C, showing that reduction of the large CuO particles mainly takes place above 200 °C. Hence, the TPR peak deconvoluted at the lower temperature can be attributed to the reduction of the fine CuO particles, which are undetectable by XRD. The amounts of copper in the fine and the large particles in Cu/$SiO_2$ are estimated from the Cu content and the peak areas in the TPR profile assuming complete reduction in the TPR experiment (see Table 3). It is noteworthy that the total quantity of the large Cu particles in the table relates roughly to the peak intensity of the XPD peak attributed to metallic copper (see Fig. 4). On the basis of the TPR result, the atomic ratios of the fine CuO particles to the large ones are calculated as 1.6, 1.0, and 0.6 for 30-, 40-, and 50-Cu/$SiO_2$, respectively. The values are significantly larger than the atomic Cu ratios of $Cu_2O$ to Cu metal determined by the Rietveld analysis on the XRD in Fig. 4 (0.3, 0.3, and 0.07, respectively). Hence, a large part of the fine particles is probably undetectable by the XRD measurement, while a part of the fine particles is detected as $Cu_2O$ after the reaction.

Assuming that all the large Cu particles in 30-Cu/$SiO_2$ are in spherical shape with a diameter of 34 nm and that the site density of Cu is 0.032 m mol $m^{-2}$ on the basis of the atomic radius, the number of Cu atoms on the surface of the large Cu particles will be only 0.07 m mol $g^{-1}$ (the density of Cu is 8.9 g $cm^{-3}$). In the cases of silica-supported catalysts prepared by the sol–gel technique, the major part of supported metallic particles is often encapsulated in the balk [7,17]. Thus, the Cu number on the metallic particle surface should be considerably larger than that of the Cu particles actually exposed on the catalyst surface.

The number of Cu atoms on the catalyst surface after the reaction can be roughly estimated from the surface atomic composition in Table 2 and the BET surface area in Table 1, assuming the site densities of $Cu^+$ as 0.058 m mol $m^{-2}$, $Si^{4+}$ as 0.35 m mol $m^{-2}$, and $O^{2-}$ as 0.030 m mol $m^{-2}$ on the basis of the ionic radii (Table 3). The value for 30-Cu/$SiO_2$ after the reaction is calculated as 0.9 m mol $g^{-1}$. Although the number of Cu atoms on the surface of the metallic Cu particles is calculated on the assumption that all the Cu particles are on the surface, the number is significantly smaller than the number of Cu atoms on the catalyst surface determined by XPS. In addition, the quantity of the fine particles is similar to that for 20-Cu/$SiO_2$ whose number of the surface Cu atoms determined by XPS is as high as 1.5 m mol $g^{-1}$ (see Table 3). Thus, it is considered that the information of the Cu $2p_{3/2}$ and Cu $L_3VV$ in the XPS for 30-Cu/$SiO_2$ originates mainly from the fine particles which are partly detected as $Cu_2O$ by XRD. In other words, the surface state of the large Cu particles is unknown by the XPS analysis. Since the $\alpha$ value suggests that the major surface species are present as $Cu^+$ (see Table 2), the XRD-invisible fine particles are also estimated to be $Cu_2O$ after the reaction; that is, the mean crystallite size of the fine $Cu_2O$ particles is considerably smaller than that determined by XRD.

The number of $Cu^+$ on the fine particle surface can be calculated as 1.3 m mol $g^{-1}$, assuming that all the fine particles in 30-Cu/$SiO_2$ are $Cu_2O$ in spherical shape with a diameter of 5 nm and that the site densities of $Cu^+$ and $O^{2-}$ are 0.058 and 0.030 m mol $m^{-2}$, respectively; the density of $Cu_2O$ is 5.9 g $cm^{-3}$. The $Cu^+$ number is probably underestimated due to the presence of the undetectable fine $Cu_2O$ particles, while a significant part of the particles are buried in the bulk.

The tendency of the Cu particle distribution on 40-Cu/$SiO_2$ is similar to that on 30-Cu/$SiO_2$, but the number of Cu atoms on the surface of 50-Cu/$SiO_2$ is fairly small and it is comparable to that of the Cu atoms on the surface of the large Cu particles (see Table 3). Hence, a certain part of the Cu atoms on the surface of 50-Cu/$SiO_2$ should belong to the metallic particles. In actual, the binding energy of Cu 2p for 50-Cu/$SiO_2$ is discernibly lower than those for 20, 30, and 40-Cu/$SiO_2$ in which the major part of the Cu atoms on the surface belong to the fine $Cu_2O$ particles (see Table 2), suggesting presence of the different Cu species from those of the fine $Cu_2O$ particles. However, the $\alpha$ value of 1849.5 eV for 50-Cu/$SiO_2$ is close to that for $Cu_2O$ [15], implying that the surface of the large metallic particles is also oxidized to $Cu^+$ during the reaction.

### 4.2. Activity of Cu/$SiO_2$

The catalytic activity of Cu/$SiO_2$ prepared by the sol–gel method increases with the Cu content up to 40 wt.%. The TPR result shows that the quantities of the fine particles ($Cu_2O$ after the reaction) in 30- and 40-Cu/$SiO_2$ are similar to that in 20-Cu/$SiO_2$ (see Table 3). It is reported that $Cu_2O$ supported on zirconium oxide is active to methanol steam reforming [18]. However, the activities of the former two catalysts are significantly higher than that of the latter. Hence, it is supposed that the large metallic Cu particles contribute significantly to the reaction although the number of Cu exposed on the surface is small. The decrease in the activity of 50-Cu/$SiO_2$ can be accounted for the decrease in the surface area of the fine $Cu_2O$ particles due to the increase in the particle size.

### 4.3. Mechanism of CO formation

The mechanism of CO formation in the methanol steam reforming has been discussed by some authors [4,19–21]. Although the direct CO formation by methanol decomposition followed by the water–gas shift reaction (WGS) has been proposed [19,20], the CO selectivities in our experiments are significantly smaller than those expected from the reaction equilibrium of WGS;

that is, the equilibrium selectivities will be 2.2% at 250 °C with the methanol conversion of 60% under the experimental conditions and 10.6% at 300 °C with the conversion of 100%. Hence, the direct CO formation is not a major reaction path of the steam reforming over $Cu/SiO_2$. Formation of methyl formate decomposed to hydrogen and carbon dioxide has been proposed as the reaction mechanism on $Cu/SiO_2$ [22]. Formation of carbon monoxide by the decomposition of methyl formate may be possible [23,24]; in the mechanism, the CO selectivity will not be greatly affected by the methanol conversion because the $CO_2$ and CO formation processes are parallel in the decomposition of methyl formate [24]. However, our experimental data show that the CO selectivity increases with an increase in the contact time, and this is in accordance with the kinetic analysis carried out by Purnama et al. in which CO formation is caused by the reverse WGS [21].

A mechanism for the reverse WGS has been proposed on copper catalysts, that is, $CO_2 + 2Cu \rightarrow CO + Cu_2O$ and $H_2 + Cu_2O \rightarrow H_2O + 2Cu$ [25]. The mechanism shows that the reaction hardly proceeds over $Cu_2O$ surface in the presence of steam and the high reactivity of Cu with steam to $Cu_2O$ may prevent CO formation. This is in agreement with the report of Ritzkopf et al. that a zirconia-supported copper catalyst gives low selectivity to carbon monoxide in methanol steam reforming and the copper surface is oxidized to $Cu^+$ state during the reaction [26]. The presence of $Cu_2O$ particles on $Cu/SiO_2$ after the reaction evidences oxidation of copper particles with steam during the reaction. On the surface of the large metallic particles, the partial oxidation of copper is hypothesized to take place as suggested by the XPS analysis with 50-$Cu/SiO_2$. Hence, the generally low CO selectivity on the $Cu/SiO_2$ catalysts may be due to the formation of $Cu^+$ species on the surface during the reaction.

The CO selectivity of 40-$Cu/SiO_2$ was decreased by the pre-reduction at 300 or 400 °C, showing that CO formation is very small both on the fine $Cu_2O$ and large metallic particles in the catalyst. Although the atomic surface concentration of copper in 40-$Cu/SiO_2$ pre-reduced at 300 or 400 °C is smaller than that for the catalyst pre-reduced at 250 °C, no significant changes in the binding energy of Cu 2p and the kinetic energy of Cu $L_3VV$ were detected (see Table 2). Hence, presence of special active sites for CO generation is suspected on 40-$Cu/SiO_2$ reduced at 250 °C and the sites may be deactivated by the reduction at 300 or 400 °C. In other words, the control factor of the CO selectivity is not simply accounted for the presence of the $Cu^+$ species on the catalyst surface. The identification of the sites for CO production is difficult even in 10 and 50-$Cu/SiO_2$, whose CO selectivities are relatively high, because such sites are still minor species on the catalysts.

When the reaction temperature is 300 °C, the CO selectivity is significantly higher than that at 250 °C. Reduction of $Cu^+$ to metal easily takes place at a high reaction temperature and it may enhance formation of CO, indicating that stabilization of $Cu^+$ species during the reaction will be important for the suppression of CO formation at 300 °C.

## 5. Conclusions

Selective methanol steam reforming to hydrogen and carbon dioxide proceeds at 250 °C over silica-supported copper prepared by a sol–gel method. When the copper content is 20 wt.% or less, copper particles are highly dispersed and oxidized to $Cu_2O$ with the mean crystallite size less than 4 nm after the reaction. Large metallic copper particles with the mean crystallite size of 30–40 nm coexist with the fine $Cu_2O$ particles in the catalyst containing 30–50 wt.% of copper after the reaction. The activity of the metallic copper particles is supposed to be higher than that of the $Cu_2O$ particles, because the surface area of the former is significantly smaller than that of the latter. The surface of the large metallic particles is estimated to be also oxidized to $Cu^+$ in the reaction at 250 °C. The presence of the $Cu^+$ species on the catalyst surface may suppress the formation of carbon monoxide by the reverse water–gas shift reaction.

## References

[1] P. Marques, N.F.P. Ribeiro, M. Schmal, D.A.G. Aranda, M.M.V.M. Souza, J. Power Sources 158 (2006) 504.
[2] C. Song, in: N. Brandon, D. Thompsett (Eds.), Fuel Cells Compendium, Elsevier, Oxford, 2005, p. 53.
[3] A. Basile, G.F. Tereschenko, N.V. Orekhova, M.M. Ermilova, F. Gallucci, A. Iulianelli, Int. J. Hydrogen Energy 31 (2006) 1615.
[4] J. Agrell, H. Birgersson, M. Boutonnet, J. Power Sources 106 (2002) 249.
[5] N. Takezawa, H. Kobayashi, A. Hirose, M. Shimokawabe, K. Takahashi, Appl. Catal. 4 (1982) 127.
[6] E.G.M. Kuijpers, R.B. Tjepkema, W.J.J. van der Wal, C.M.A.M. Mesters, S.F.G.M. Spronck, J.W. Geus, Appl. Catal. 25 (1986) 139.
[7] Z. Wang, Q. Liu, J. Yu, T. Wu, G. Wang, Appl. Catal. A 239 (2003) 87.
[8] Y.-M. Lin, M.-H. Rei, Catal. Today 67 (2001) 77.
[9] F. Izumi, T. Ikeda, Mater. Sci. Forum 321–324 (2000) 198.
[10] ISO 18118 (2004).
[11] JCPDS Files, 40836, 50667, and 410254.
[12] C. Hammond, The Basics of Crystallography and Diffraction, Oxford University Press, New York, 1997, p. 145.
[13] J.W.E. Coenen, Appl. Catal. 75 (1991) 193.
[14] Y. Matsumura, K. Kuraoka, T. Yazawa, M. Haruta, Catal. Today 45 (1998) 191.
[15] C.D. Wagner, Practical surface analysis,, in: D. Briggs, M.P. Seah (Eds.), second edition, Auger and X-ray Photoelectron Spectroscopy, vol. 1, John Wiley & Sons, Inc., New York, 1990, p. 595.
[16] Y. Matsumura, T. Nakamori, Appl. Catal. A 258 (2004) 107.
[17] Y. Matsumura, N. Tode, T. Yazawa, M. Haruta, J. Mol. Catal. A 99 (1995) 183.
[18] H. Oguchi, H. Kanai, K. Utani, Y. Matsumura, S. Imamura, Appl. Catal. A 293 (2005) 64.
[19] E. Santacesaria, S. Carrà, Appl. Catal. 5 (1983) 345.
[20] B.A. Peppley, J.C. Amphlett, L.M. Kearns, R.F. Mann, Appl. Catal. A 179 (1999) 31.
[21] H. Purnama, T. Ressler, R.E. Jentoft, H. Soerijanto, R. Schlögl, R. Schomäcker, Appl. Catal. A 259 (2004) 83.
[22] K. Takahashi, N. Takezawa, H. Kobayashi, Appl. Catal. 2 (1982) 363.
[23] T.P. Minyukova, I.I. Simentsova, A.V. Khasin, N.V. Shtertser, N.A. Baronskaya, A.A. Khassin, T.M. Yurieva, Appl. Catal. A 237 (2002) 171.
[24] Y. Choi, H.G. Stenger, Appl. Catal. B 38 (2002) 259.
[25] M.J.L. Ginés, A.J. Marchi, C.R. Apesteguía, Appl. Catal. A 154 (1997) 155.
[26] I. Ritzkopf, S. Vukojević, C. Weidenthaler, J.-D. Grunwaldt, F. Schüth, Appl. Catal. A 302 (2006) 215.